coatings

MDPI

Article

Wear Characteristics of Textured Floating Oil Seal Surfaces: A Simulation and Experimental Study

Hailin Zhao [1], Guilin Li [1], Zhaoyang Zhai [2,*], Jialin Yang [2], Dongya Zhang [2] and Yanchao Zhang [2]

[1] TaiHang Laboratory, Chengdu 610000, China; zhaohailin@mail.nwpu.edu.cn (H.Z.); guilin_li2024@163.com (G.L.)
[2] School of Mechanical and Precision Instrument Engineering, Xi'an University of Technology, Xi'an 710048, China; yjlbisheng@163.com (J.Y.); dyzhang@xaut.edu.cn (D.Z.); zhangyanchao@xaut.edu.cn (Y.Z.)
* Correspondence: zyzhai@xaut.edu.cn

Abstract: This study aimed to analyze the effects of surface texture on the wear amount of floating oil seals and how these effects are related to the texture parameters. To achieve this, a finite element model was constructed to simulate the frictional behavior of seal discs under both textured and non-textured conditions. The study focused on a specific set of texture parameters. The texture depth was held constant, while the area density and diameter of the textures were varied. Three different area densities were considered: 10%, 20%, and 30%. Similarly, three different texture diameters were included in the study: 100, 200, and 300 μm. For each combination of area density and diameter, three different texture depths were evaluated: 50, 100, and 150 μm. The results show that compared with the non-texture, the wear loss of the texture is significantly reduced, and the wear loss is reduced by 56.8%. As the texture depth increases, the corresponding increase in wear remains relatively small. In contrast, increasing the texture diameter and area density leads to a more significant increase in wear, indicating that these two parameters have a more significant effect on the wear behavior of the seal. Under the condition of dry friction, the average friction coefficient analysis shows that the texture area density is 30%, the texture diameter is 200 μm, and the minimum value is about 0.602. Under the lubrication condition, the lowest average friction coefficient is about 0.147, the texture area density is 20%, and the texture diameter is 300 μm.

Keywords: sprocket assembly; finite element model; surface texture; wear amount

Citation: Zhao, H.; Li, G.; Zhai, Z.; Yang, J.; Zhang, D.; Zhang, Y. Wear Characteristics of Textured Floating Oil Seal Surfaces: A Simulation and Experimental Study. *Coatings* **2024**, *14*, 1087. https://doi.org/10.3390/coatings14091087

Academic Editor: Manuel António Peralta Evaristo

Received: 15 July 2024
Revised: 2 August 2024
Accepted: 4 August 2024
Published: 24 August 2024

1. Introduction

As one of the key components of scraper conveyor, the sealing performance of the floating oil seal is very important for the normal operation of the equipment [1–3]. However, in practical applications, due to factors such as the long-term working environment and the quality of the material itself, wear and leakage problems often occur in floating oil seals, resulting in a decrease in overall performance and an increase in maintenance costs. Therefore, how to improve the service life and reliability of floating oil seals has become one of the key technical problems to be solved urgently. In view of this, the researchers further proposed a surface texture construction strategy based on optimization design [4]. Through the precise control of the surface microstructure, the wear resistance of the sprocket surface can be effectively enhanced, and the texture wear rate can be reduced, thereby improving the service life and operational reliability of the whole machine.

The design and fabrication of surface textures have represented an effective method for improving the wear resistance of materials [5–9]. By creating micro-scale structures on material surfaces, surface texture technology enhances the friction coefficient and lubrication effect, thereby achieving wear resistance. Studies have demonstrated that the primary wear-reduction mechanisms of surface textures involve increasing oil film thickness, increasing contact area, and reducing surface roughness [10,11]. Surface texture

technology has found widespread applications in various mechanical equipment and industrial sectors, such as automotive, aerospace, marine, and rail transit [12–16]. A deeper understanding of the mechanisms behind surface texture can facilitate its wider adoption in industrial settings. For instance, Yan et al. [17] conducted simulation analyses to evaluate the effectiveness and influencing factors of floating seals in sprocket assembly, with experimental validation. Their findings indicated that floating seals effectively reduce wear and oil leakage in sprocket assemblies, finally improving sealing performance and operational efficiency. Through combined simulation and experimental investigations, Wang [18] proposed that the contact pressure between the floating seal ring and the shaft surface significantly affects sealing performance. Factors such as the axial stiffness of the sealing ring, lubricant film thickness, and axial displacement also affect sealing effectiveness. Lee et al. [19] experimentally demonstrated that seal leakage and service life are influenced by various factors, including lubrication conditions and axial displacement. They suggested structural optimization and material replacement as strategies to reduce friction and wear, thereby enhancing floating seal performance. Focusing on the wear mechanisms of sprocket assemblies, Grill et al. [20] analyzed the wear characteristics and influencing factors of sprocket assembly. They proposed a series of maintenance strategies, including the application of floating seals, regular lubrication, and the replacement of worn parts, to enhance operational efficiency and prolong service life.

In this study, the influence mechanism of surface texture on friction behavior was deeply analyzed by comparing the finite element simulation of textured and untextured surfaces [21–25]. The wear amount in the simulation was extracted and compared with the friction experimental data. The effects of surface texture on friction coefficient curve, average friction coefficient, wear rate and wear surface morphology were comprehensively explored. For engineering applications such as sprocket assembly, the research also optimizes the depth, diameter and density parameters of the circular texture structure. Through the combination of simulation analysis and experimental verification, the best texture design that can improve the service life and performance of the equipment and reduce the maintenance cost is obtained. This has achieved effective optimization for engineering applications and provided theoretical support for related technological progress.

2. Materials and Methods

This research employed an Rtec MFT-5000 friction and wear testing machine from NanJing to conduct tribological experiments. The instrument is known for its advanced capabilities and robust stability, enabling it to offer reliable tribological properties and parameters of materials. Besides, the machine is equipped with an optical system for observing and recording the morphological characteristics of the worn surfaces.

In this paper, laser processing was used to manufacture surface texture. The laser processing instrument used was LR-Fib-30T from Xi'an Langrui company, the wavelength was 1064 nm, and the maximum output power was 60 W. By adjusting the parameters such as laser power, scanning speed and scanning spacing, textures with different depths and scales can be fabricated on the surface of the workpiece. Through repeated tests and measurements, the best processing parameters are obtained: laser power 7.2 W, laser frequency 25 kHz, processing speed 200–250 mm/s.

In the design and optimization of floating seals, lateral pressure, friction coefficient and material hardness are three key parameters. Compared with other rubber materials, nitrile rubber has good performance and low friction coefficient. Therefore, nitrile rubber was selected as the research object in this study.

In this paper, the circular texture is selected for research, and the texture distribution is as shown in Figure 1c. The main reasons are as follows: the circular texture can reduce the contact area, thereby reducing the wear of the friction element. At the same time, it can form a small space on the contact surface, which is conducive to the storage of lubricants, plays a lubricating role, and reduces the friction coefficient. In addition, the circular structure

can better capture and embed particles or droplets, which is very important in some applications. Finally, it has excellent anti-adhesion and can keep the surface clean.

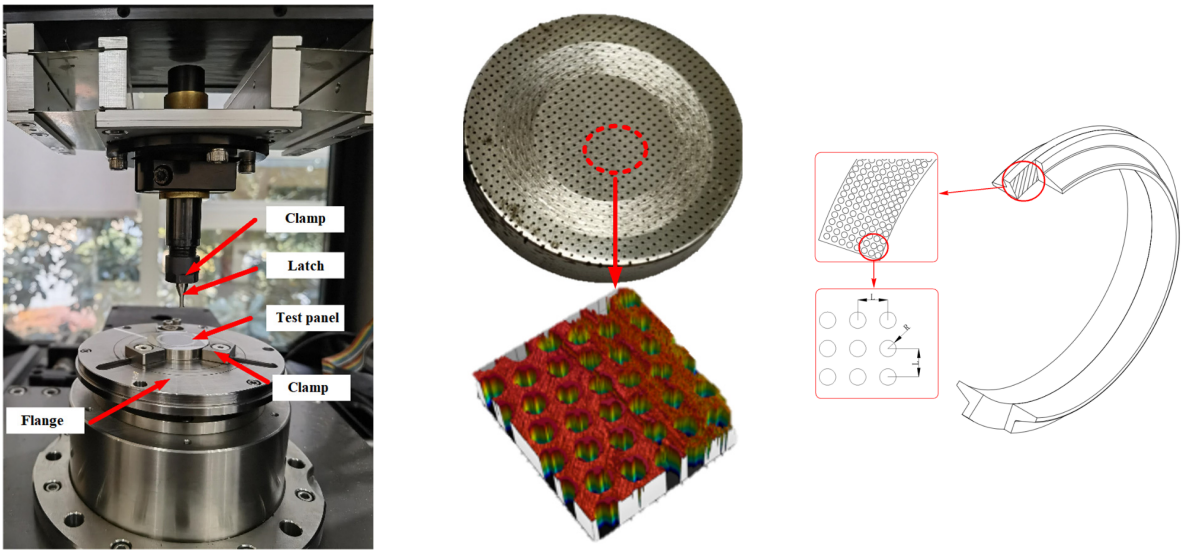

(**a**) Rtec MFT-5000 friction and wear tester (**b**) Test panel after friction test and pattern morphology scanning diagram (**c**) Surface texture distribution

Figure 1. The friction and wear testing machine utilized in this study, along with a representative image of the wear track on a tested sample and surface texture distribution diagram: (**a**) Rtec MFT-5000 friction and wear tester; (**b**) Test panel after friction test and pattern morphology scanning diagram; (**c**) Surface texture distribution.

To simulate the working conditions of a floating oil seal, a pin-on-disc configuration was chosen for the rotary sliding friction analysis. The pin, with a diameter of 4 mm, was set to slide against a disc with a diameter of 30 mm and a thickness of 5 mm. The wear track radius for the experiment was set at 10 mm. The study evaluated the tribological behavior of materials with varying surface textures. Specifically, three different surface densities (10%, 20%, and 30%) and three different texture diameters (100, 200, and 300 μm) were examined. The texture depth was kept constant at 100 μm for all experiments.

The simulation models are simplified into finite element models with and without surface texture based on whether surface texture is added. The finite element model with surface texture incorporates a woven texture with a diameter of 200 μm, a depth of 100 μm, and an areal density of 20% for simulation calculations. The specific parameters of the model are as follows: the cylindrical pin has a radius of 2 mm and a height of 5 mm, while the flat bottom plate has a thickness of 2 mm, a length of 62.8 mm, and a width of 4 mm.

In this paper, the Archard wear model is used to simulate the friction and wear phenomena on the metal surface. Archard wear model is an empirical model widely used in friction and wear analysis of metal surfaces [26,27]. The basic formula is:

$$W = \frac{K(T)}{H(T)} \int pv\mathrm{d}t \tag{1}$$

In the formula, W is the wear value; $K(T)$ is the material characteristic function; $H(T)$ is the material hardness function; p is the pressure on the surface of the structure; v is the flow velocity of material plastic deformation along the surface of the structure; T is the initial temperature of the structure.

The basic principle of the model is that the friction effect of the contact surface will gradually smooth the surface micro-protrusions, resulting in surface area changes and protrusion reduction, thereby increasing the contact stress per unit area and increasing the

friction force. The Archard model is widely used in the analysis and design of mechanical systems in the field of material science and engineering, such as bearings, gears, and cutting tools. It can also be used to study different types of wear mechanisms, such as abrasive wear, surface fatigue wear, and corrosion wear.

The simulation utilizes Archard's wear model to simulate the friction and wear phenomena on metal surfaces. A transient analysis with a time step of 0.0001 s and a total simulation time of 0.5 s is employed. The contact calculation adopts a pure penalty function algorithm. To address the discrepancy between the initial stiffness matrix calculation and the actual situation caused by deformation of the worn surface, a large deformation setting is enabled, allowing the stiffness matrix to be iteratively calculated with structural deformation. To simulate the kinematic behavior of the pin-on-disc tribometer, a hinge constraint is applied to the cylindrical pin, restricting its motion in the X and Z directions while allowing free movement in the Y direction. The flat bottom plate is fixed in all directions. The relative frictional motion of the pin is simulated by the transverse movement of the disc. A compressive load is applied in the negative Y direction, ensuring sufficient contact force between the cylindrical pin and the flat bottom plate to generate friction.

To ensure simulation accuracy, the PV value of the simulation model needs to be consistent with the actual working conditions. The specific values are demonstrated in the table below. The calculated similarity ratio between the PV value of the actual model (Table 1) and that of the simulation model (Table 2) is 98.3%, which is in the permissible error range, demonstrating the effectiveness of the calculation method utilized in this paper.

Table 1. PV values from pin-on-disk friction tests.

Load (N)	Pin Radius (mm)	Rotational Speed (r/min)	Contact Pressure (MPa)	Linear Velocity (m/s)	PV Value ($MPa \cdot m \cdot s^{-1}$)
4	2	1200	0.318	1.256	0.399

Table 2. PV values from finite element model.

Load (N)	Contact Stress (MPa)	Velocity (m/s)	PV Value ($MPa \cdot m \cdot s^{-1}$)
4	0.318	1.3	0.413

3. Results

3.1. Analysis of Wear Scar Patterns on the Model

The presence of surface texture plays a crucial role in reducing wear on the oil seal seat. However, the diameter, density, and depth of the surface texture significantly affect its wear reduction efficiency. To better understand the effect of surface texture on wear, simulations were conducted on surfaces with and without surface textures, each with varying parameters.

Figures 2 and 3 illustrate the wear scar patterns at corresponding times for surfaces without and with surface texture, respectively. A comparison indicates that wear amount increases over time, and the wear region is primarily concentrated on the outer ring in the presence of the surface texture. Figures 2f and 3f respectively show the maximum wear amount of the textureless structure and the maximum wear amount of the textured structure, which are 4.77×10^{-9} and 8.98×10^{-10} mm^3, respectively. This indicates that applying a surface texture treatment to the surface can effectively reduce the wear amount of the workpiece. These findings highlight the effect of surface texture on wear distribution. The introduction of textures changes the wear distribution, leading to a more dispersed pattern once stabilized.

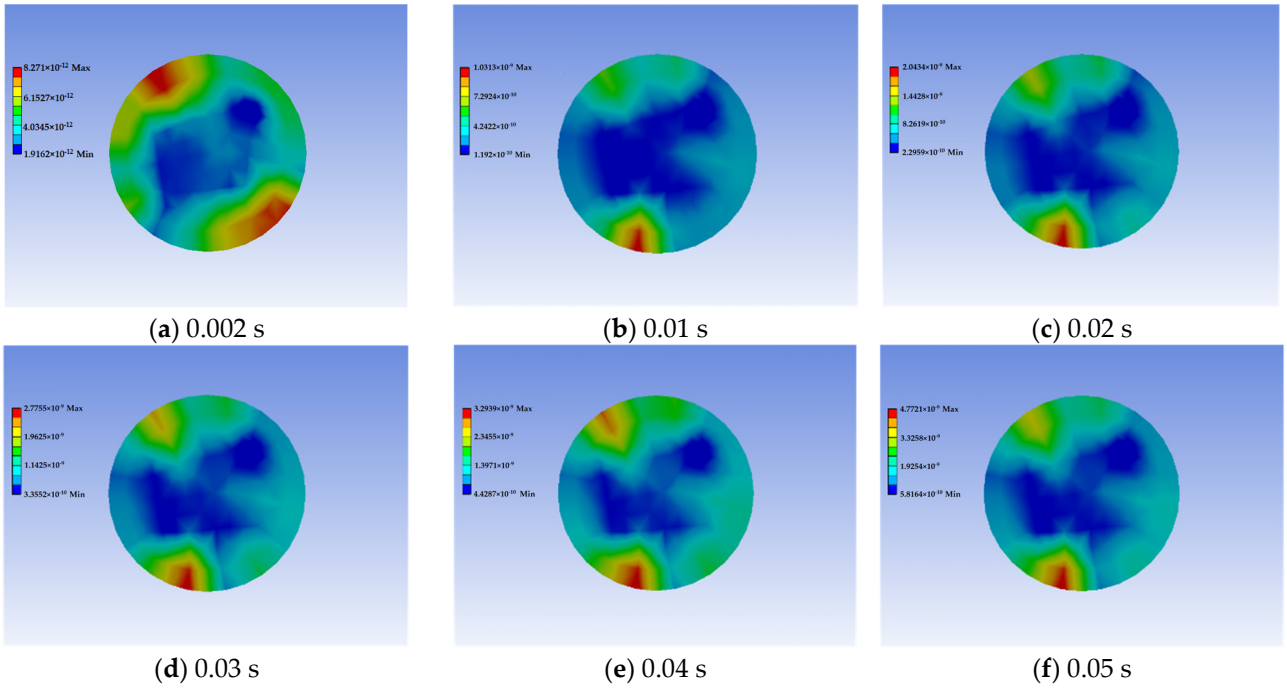

(**a**) 0.002 s (**b**) 0.01 s (**c**) 0.02 s

(**d**) 0.03 s (**e**) 0.04 s (**f**) 0.05 s

Figure 2. Wear scar patterns of the pin without surface texture at different time points: (**a**) 0.002 s; (**b**) 0.01 s; (**c**) 0.02 s; (**d**) 0.03 s; (**e**) 0.04 s; (**f**) 0.05 s.

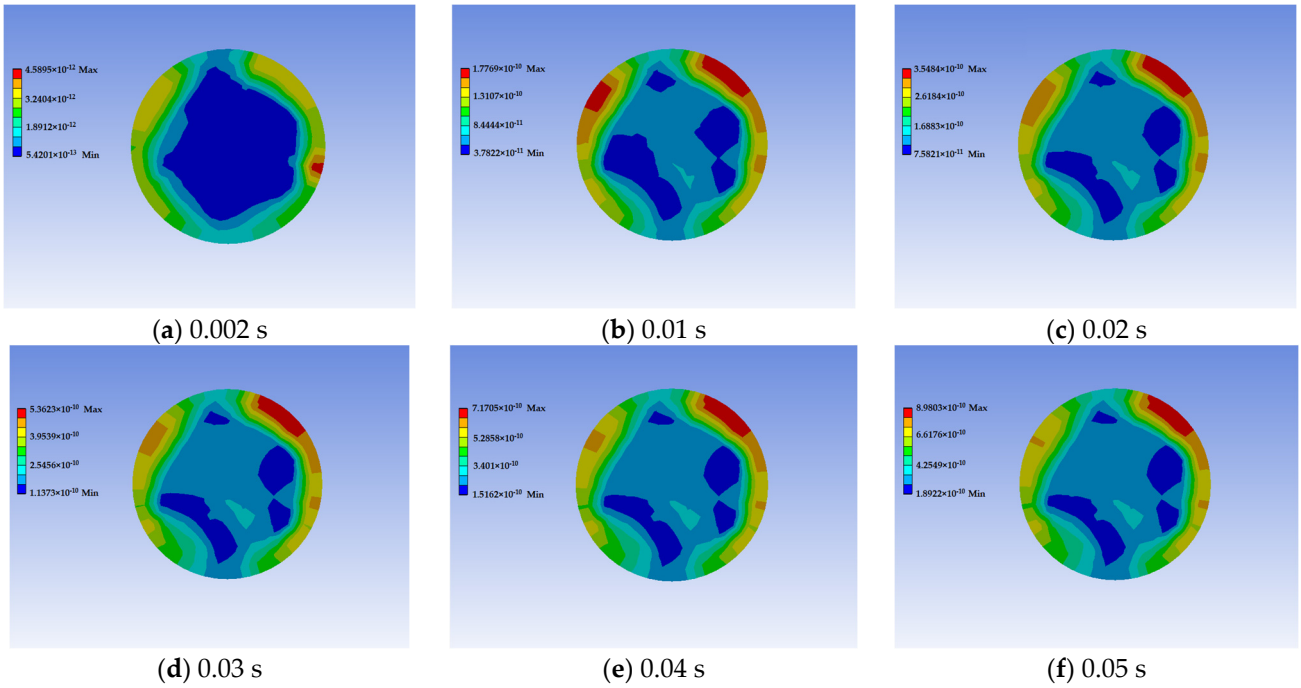

(**a**) 0.002 s (**b**) 0.01 s (**c**) 0.02 s

(**d**) 0.03 s (**e**) 0.04 s (**f**) 0.05 s

Figure 3. Wear scar patterns of the pin with surface texture at different time points: (**a**) 0.002 s; (**b**) 0.01 s; (**c**) 0.02 s; (**d**) 0.03 s; (**e**) 0.04 s; (**f**) 0.05 s.

A comparative analysis was conducted on the wear patterns of a non-textured flat endplate (Figure 4) and a textured flat endplate (Figure 5) at corresponding time intervals. The data shows that the wear volume of the non-textured surface increased significantly from 4.59×10^{-12} mm^3 in Figure 4a to 1.22×10^{-9} mm^3 in Figure 4f. In contrast, the wear volume range for the textured surface was from 1.15×10^{-12} mm^3 in Figure 5a to 3.68×10^{-10} mm^3 in Figure 5f, with wear mainly concentrated on the left side. Specifically, while both surfaces exhibited similar overall wear trends, the presence of surface texture

significantly changed the distribution of wear. These findings highlight the influential role of surface texture on wear distribution. The introduction of surface texture causes wear to be primarily localized around the textured grooves. This phenomenon is attributed to the change of material surface stress distribution by the texture. Moreover, over time, the area of most severe wear consistently remained concentrated on the left side.

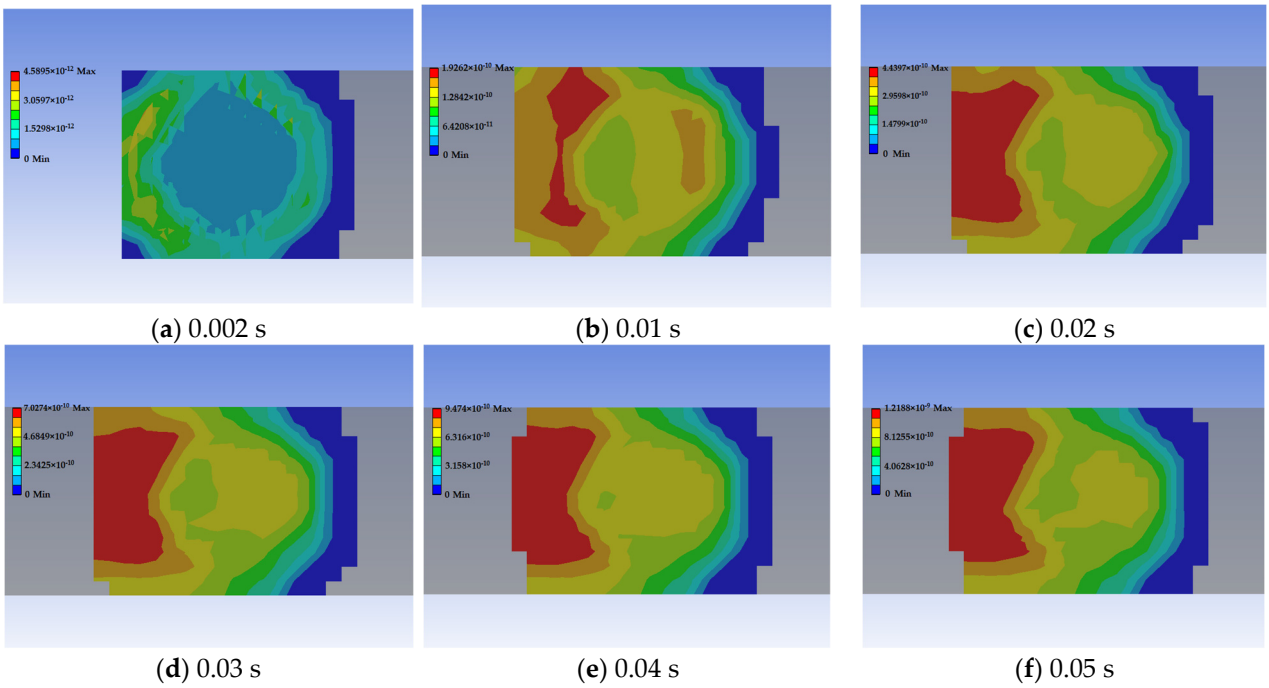

(**a**) 0.002 s (**b**) 0.01 s (**c**) 0.02 s

(**d**) 0.03 s (**e**) 0.04 s (**f**) 0.05 s

Figure 4. Wear pattern of the flat endplate without surface texture at different time points: (**a**) 0.002 s; (**b**) 0.01 s; (**c**) 0.02 s; (**d**) 0.03 s; (**e**) 0.04 s; (**f**) 0.05 s.

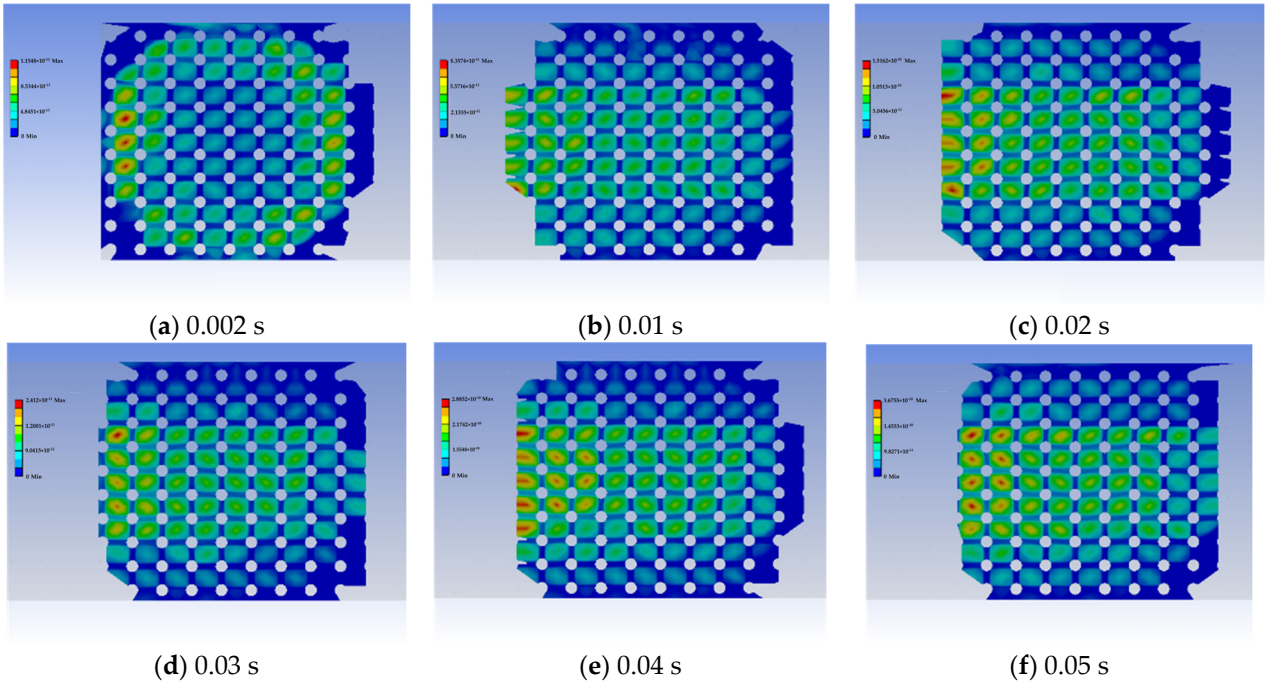

(**a**) 0.002 s (**b**) 0.01 s (**c**) 0.02 s

(**d**) 0.03 s (**e**) 0.04 s (**f**) 0.05 s

Figure 5. Wear pattern of the flat endplate with surface texture at different time points: (**a**) 0.002 s; (**b**) 0.01 s; (**c**) 0.02 s; (**d**) 0.03 s; (**e**) 0.04 s; (**f**) 0.05 s.

Figure 6a illustrates the temporal change of average wear amount extracted from all nodes on the pin contact surface. As depicted, the average wear amount across the entire friction surface of the pin exhibits an approximately linear increase over time. According to Archard's wear law and its generalized form, wear amount is directly proportional to contact pressure and sliding distance. While the contact pressure distribution on the pin friction surface is not uniform, the gradient of contact pressure remains relatively insignificant once stabilized; in contrast, sliding distance increases linearly with time. Therefore, the resulting wear amount finally displays a largely linear increasing trend.

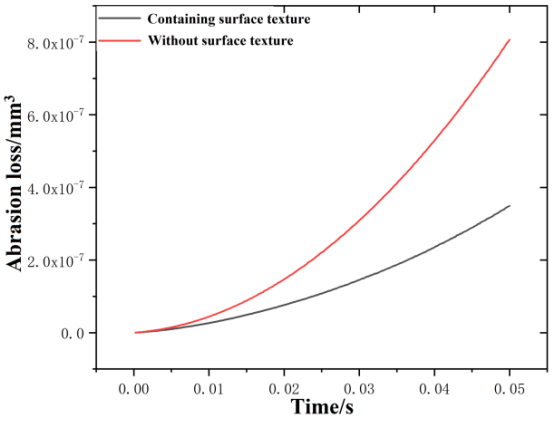

(**a**) Wear curves with and without surface weave

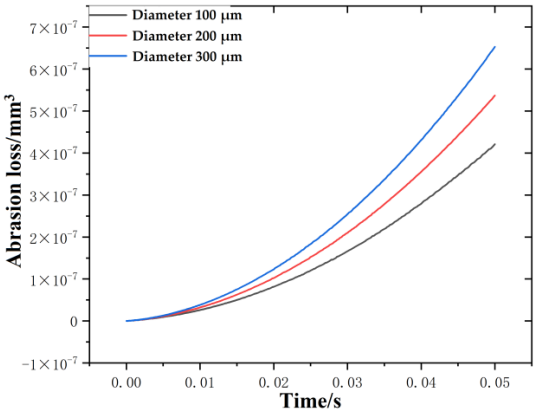

(**b**) Wear curves corresponding to different texture diameters

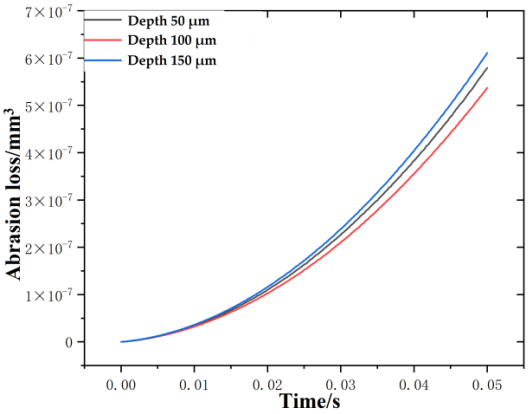

(**c**) Wear curves corresponding to different texture depths

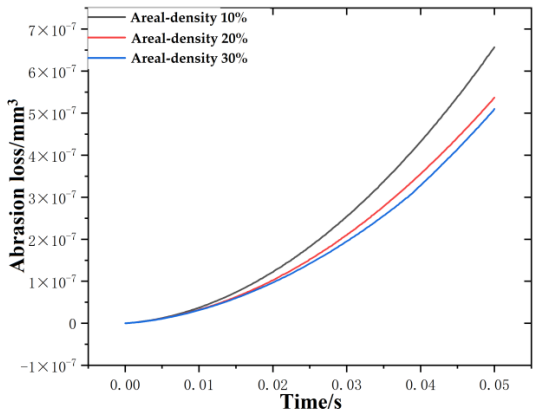

(**d**) Wear curves corresponding to different texture surface density

Figure 6. Fitted curves of wear amount under different conditions: (**a**) Wear curves with and without surface weave; (**b**) Wear curves corresponding to different texture diameters; (**c**) Wear curves corresponding to different texture depths; (**d**) Wear curves corresponding to different texture surface density.

The presence of surface texture plays a crucial role in reducing wear on the oil seal seat. Specifically, the diameter, density, and depth of the surface texture significantly affect its wear reduction efficiency. Therefore, to gain a more comprehensive understanding of the effect of surface texture on wear, simulations were conducted utilizing various texture diameters, depths, and area densities.

Figure 6 presents the simulation results of wear analysis. It is evident that the wear amount is relatively small when the texture diameter ranges from 100 to 200 μm. However, as the texture diameter increases from 100 to 300 μm, a significant difference in wear amount appears, reaching up to 2.4×10^{-7} mm^3. This observation suggests that the texture diameter has a significant effect on wear behavior. Regarding texture depth, a depth of

100 μm yields the minimum wear amount. In addition, when the texture depth varies between 50 and 150 μm, the wear amount difference reaches 0.95×10^{-7} mm^3. This indicates that, compared to texture diameter, the effect of texture depth on wear is relatively minor. Analyzing the effect of texture area density, it becomes apparent that a density between 20% and 30% results in lower wear. In the range of 10% to 30% texture area density, the wear amount difference reaches 1.41×10^{-7} mm^3, highlighting a significant effect of texture area density on wear performance. Specifically, a higher texture area density can enhance lubrication conditions and reduce the friction coefficient, effectively reducing wear. Therefore, to achieve optimal wear control, a texture depth of 100 μm, an area density between 20% and 30%, and a diameter ranging from 100 to 200 μm are determined to be the most effective parameters for surface texture.

3.2. Research on the Friction Mechanism of Floating Oil Seals in Sprocket Assemblies

This study evaluates the wear characteristics and mechanisms of floating oil seals in sprocket assemblies under different texture parameters. Researchers utilized a surface texture friction mechanism experiment to evaluate the wear reduction effects of surface textures. They conducted centerless grinding and surface texture wear tests on the material surface to study the friction and wear properties of different texture parameter combinations under oil-lubricated and dry friction conditions. The evaluation and selection of texture parameter combinations with excellent performance were based on factors such as friction coefficient, average friction coefficient, surface morphology, and wear rate.

The analysis of the friction and wear characteristics of the surface texture on this material was conducted under both dry friction and oil lubrication conditions. Figure 7 illustrates the surface morphology of the test disc under dry friction test conditions. As depicted, the disc with a texture diameter of 100 μm exhibits minimal wear marks. With an increase in texture diameter, the wear marks become progressively more evident. This phenomenon can be attributed to the change of surface stress distribution by the surface texture. Larger texture diameters primarily contribute to a cutting wear mechanism. This is because larger diameter surface textures tend to create wider gaps, facilitating the movement of abrasives and particles between surfaces.

(**a**) 20%–100 μm (**b**) 20%–200 μm (**c**) 20%–300 μm

Figure 7. Morphology of each test disc under dry friction conditions: (**a**) 20%–100 μm; (**b**) 20%–200 μm; (**c**) 20%–300 μm.

To better understand how texture parameters affect wear amount, a series of experiments were conducted. The wear amounts corresponding to different texture parameters are presented in Table 3. Specifically, the wear rate for texture parameters of 20%–200 μm demonstrates a 7.2% deviation from the simulation results discussed earlier.

Table 3. Wear amount for different weaving parameters.

No.	Texture Parameters	Wear Amount (mm^3)	Wear Rate (10^{-6} mm^3/N·m)
1	10%–100 μm	0.0082	1.82
2	10%–200 μm	0.0108	2.39
3	10%–300 μm	0.0096	2.12
4	20%–100 μm	0.0105	2.33
5	20%–200 μm	0.0116	2.57
6	20%–300 μm	0.0124	2.75
7	30%–100 μm	0.0137	3.04
8	30%–200 μm	0.0126	2.79
9	30%–300 μm	0.0112	2.48

It is well established that appropriate surface texture can affect the coefficient of friction (COF), either increasing or decreasing it. To study the tribological behavior of surface texture on this specific material, friction experiments were conducted under dry friction conditions, adhering to the parameters outlined in previous section, The resulting COF over time is depicted in Figure 8.

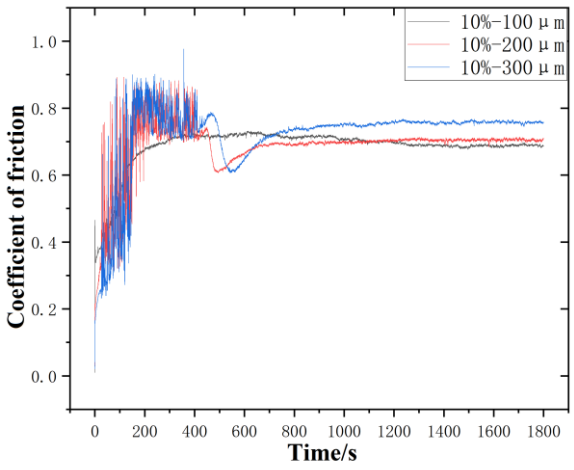

(**a**) Different diameters at 10% areal density

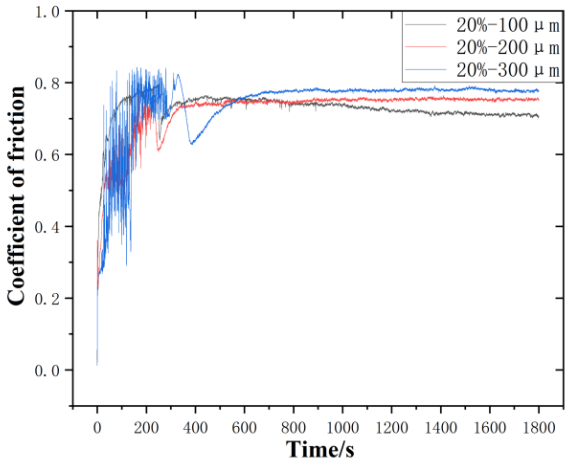

(**b**) Different diameters at 20% areal density

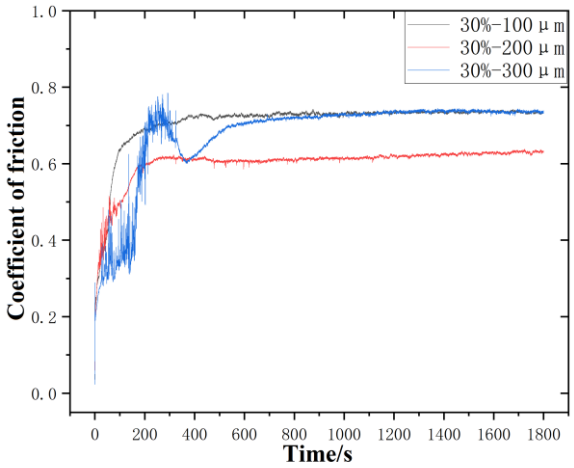

(**c**) Different diameters at 30% areal density

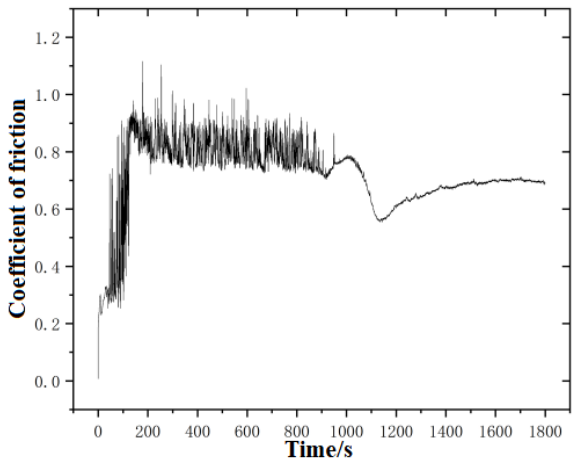

(**d**) Centerless grinding treatment

Figure 8. Friction coefficient curves for different diameters with the same density under dry friction conditions: (**a**) Different diameters at 10% areal density; (**b**) Different diameters at 20% areal density; (**c**) Different diameters at 30% areal density; (**d**) Centerless grinding treatment.

When comparing friction coefficients across the same diameter, observe a consistent trend at surface densities of 10% and 20%. Specifically, the coefficient of friction for a 100 μm diameter decreases in the latter half of the experiment. However, this trend reverses at a 30% surface density, indicating that in the 100 μm diameter range, friction coefficients increase proportionally with surface density. Further analysis indicates that at 10% and 20% surface densities, a larger friction coefficient is observed for a 200 μm diameter. This coefficient decreases significantly when the surface density reaches 30%, whereas, at a 300 μm diameter, the friction coefficient remains relatively stable across all three surface densities.

To better understand the morphological characteristics of the surface texture post-treatment, we selected samples with a fixed texture diameter and varying surface densities. Figure 9 illustrates the wear patterns observed on a portion of the disc, where one can clearly observe a reduction in wear as the surface texture density increases.

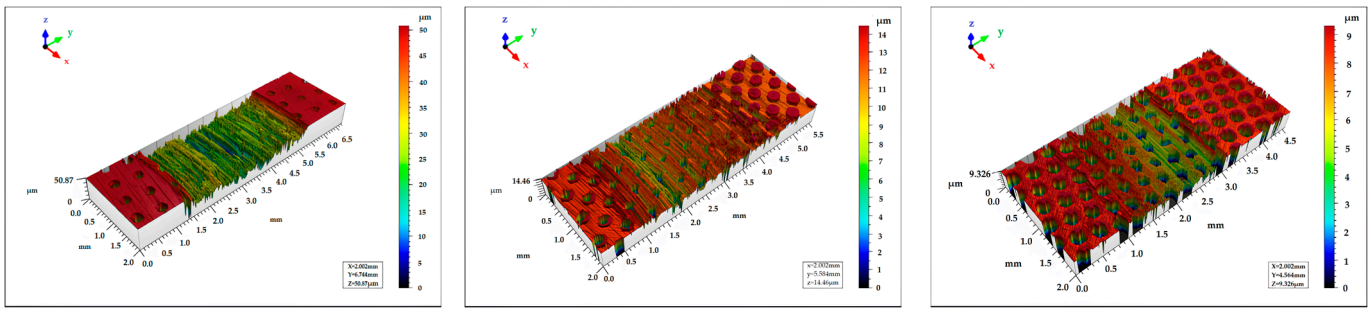

(**a**) 0%–200 μm (**b**) 20%–200 μm (**c**) 30%–200 μm

Figure 9. Wear morphology of surface weaving at different surface densities: (**a**) 10%–200 μm; (**b**) 20%–200 μm; (**c**) 30%–200 μm.

Finally, the length of the test pins was measured and compared, yielding the data presented in Table 4. As demonstrated in the table, the average wear length of the textured test pins is 0.24 mm. This represents a 0.76 mm reduction in wear amount compared to the untextured samples.

Table 4. Wear of the length of test pins at different parameters.

Surface Density \ Texture Diameter (μm)	100	200	300
10%	25.9 mm	25.64 mm	25.56 mm
20%	25.8 mm	25.8 mm	25.72 mm
30%	25.8 mm	25.8 mm	25.8 mm

Figure 10 illustrates the surface morphology of the test disks under lubricated conditions. As evident from the figure, there are no significant wear marks on the surfaces of the disks. This highlights the significant wear reduction effect of the various texture parameters. This positive effect is attributed to the texture's ability to retain a small amount of lubricating oil, which forms a lubricating film during friction. Besides, the texture itself can trap a small amount of wear debris. Only on the surface with texture parameters of 20%–100 μm can slight wear marks be observed.

Tribological tests were conducted under oil lubrication conditions as outlined in previous section, and the resulting friction coefficient over time is demonstrated in Figure 11. It is evident that at surface densities of 10% and 20%, the friction coefficient is minimized when the texture diameter is 300 μm. Therefore, under oil lubrication conditions, surface textures with larger area densities are preferable. This is because a larger area density allows for a greater amount of lubricating oil to be retained, thereby reducing the friction coefficient. At a surface density of 30%, the surface texture with a diameter of 200 μm exhibits the lowest friction coefficient.

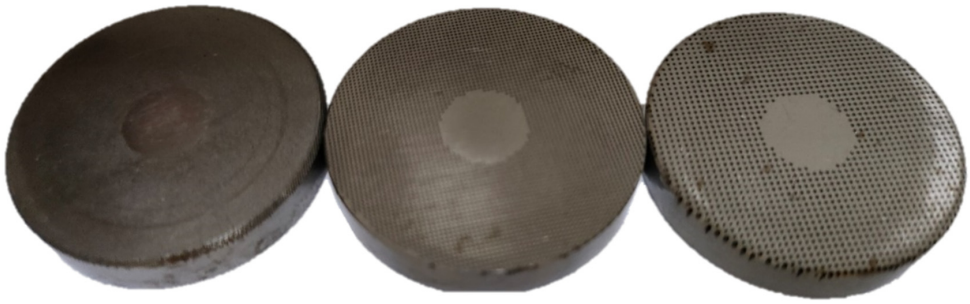

(**a**) 20%–100 μm (**b**) 20%–200 μm (**c**) 20%–300 μm

Figure 10. Morphology of each test disc under oil lubrication condition: (**a**) 20%–100 μm; (**b**) 20%–200 μm; (**c**) 20%–300 μm.

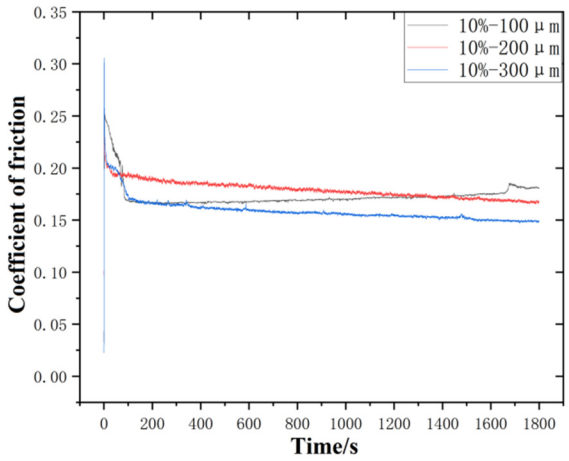

(**a**) Different diameters at 10% areal density

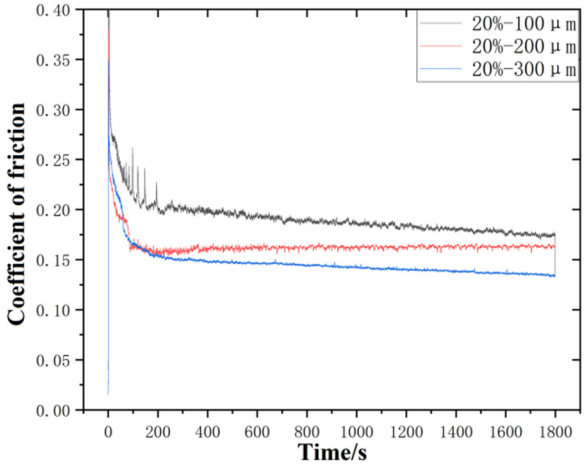

(**b**) Different diameters at 20% areal density

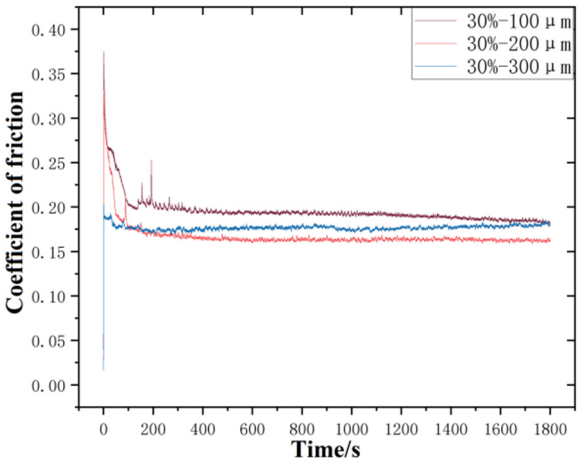

(**c**) Different diameters at 30% areal density

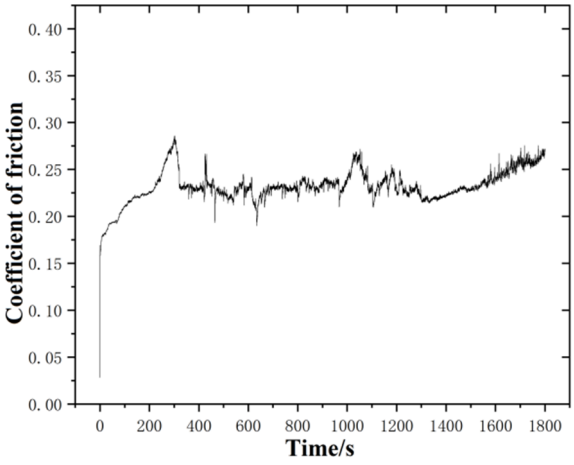

(**d**) Centerless grinding treatment

Figure 11. Friction coefficient curves for different diameters with the same density under oil lubrication conditions: (**a**) Different diameters at 10% areal density; (**b**) Different diameters at 20% areal density; (**c**) Different diameters at 30% areal density; (**d**) Centerless grinding treatment.

Table 5 shows the wear of the test pin under different parameters. The average friction coefficient for each of the nine test conditions was calculated and plotted in Figure 11. As can be seen, the lowest average friction coefficient of 0.147 is achieved with a surface

density of 20%. Therefore, the optimal surface texture for this application is a diameter of 300 μm and a surface density of 20%.

Table 5. Wear of test pins at different parameters.

Surface Density \ Texture Diameter (μm)	100	200	300
10%	25.92 mm	25.92 mm	25.8 mm
20%	25.88 mm	25.84 mm	25.82 mm
30%	25.88 mm	25.84 mm	25.9 mm

4. Discussion

This study first established finite element simulation models for both pin-on-disc specimens with surface textures and those without. The simulation results were then compared with experimental results. The study demonstrates that wear on the cylindrical pin surfaces increases as time passes, and the wear is mainly distributed on the outer circumference. By comparing the wear amounts of the two models, it is found that the wear amount with surface textures is reduced by 56.8% compared with that without surface textures. This is basically consistent with the existing research results [5–8]. It is worth noting that this study found that with the increase of texture depth, the wear increment is smaller, which further confirms the effectiveness of surface texture in reducing the wear of mechanical pairs. It shows that the correlation between texture depth and wear is low. This is different from the research results of Palafox et al. [5,8]. They found that texture depth is an important parameter affecting wear. The possible reasons for this difference are differences in material properties; different friction environment; and differences in experimental methods and measurement methods. Therefore, when optimizing the surface texture parameters, it is necessary to fully consider the actual application conditions. In addition, this study also found that texture diameter and area density have a significant effect on wear. This is basically consistent with the research results of Wang et al. [22]. They also found that reasonable selection of texture parameters can achieve the best tribological performance. However, there are still differences in the specific values between the two, which may be due to the differences in test conditions and material systems.

In addition, centerless grinding and surface texture wear tests were conducted to study the friction and wear properties of different texture parameter combinations under oil-lubricated and dry friction conditions. The friction coefficient, average friction coefficient, surface morphology, and wear rate were utilized to evaluate and select the texture parameter combinations with excellent performance. Studies have demonstrated that under dry friction conditions, the friction test runs well and stably and can be utilized for the following experimental studies. Under oil-lubricated conditions, due to the presence of the oil film, the wear amount and friction coefficient are both reduced. In the study of textured wear characteristics, it is learned through the analysis of the average friction coefficient that when the area density is 30% and the texture diameter is 200 μm, the friction coefficient is the smallest; under oil lubrication conditions, through the joint analysis of experiments and simulations, it is known that when the area density is 20% and the texture diameter is 300 μm, the best friction reduction and wear reduction effect are obtained.

5. Conclusions

In summary, the wear of the pin surface increases with time and is mainly concentrated on the outer circle. The wear loss of the textured surface is 56.8% less than that of the non-textured surface. By using the control variable method, it is found that the texture depth has little effect on wear, and the texture diameter and surface density have great influence on wear. Through experimental verification, it is found that under dry friction conditions, the friction coefficient is the smallest when the surface density is 30% and the texture diameter is 200 μm. Under oil lubrication conditions, the friction coefficient is the smallest when the surface density is 20% and the texture diameter is 300 μm. Therefore,

texture parameters should be selected as follows: surface density 30% diameter 200 μm or 20% deep diameter 300 μm.

Author Contributions: Conceptualization, Methodology, Writing-Original draft preparation, H.Z.; Visualization, Editing, G.L.; Investigation, Z.Z.; Data curation, J.Y.; Supervision, D.Z.; Reviewing, Y.Z.; All authors have read and agreed to the published version of the manuscript.

Funding: This research was funded by National Natural Science Foundation of China (52075436), Key Research and Development Program of Shaanxi (2024GX-YBXM-216, 2024GX-YBXM-284), China Postdoctoral Science Foundation (2023M743246).

Institutional Review Board Statement: Not Applicable.

Informed Consent Statement: Not Applicable.

Data Availability Statement: The datasets generated and/or analyzed during the current study are available from the corresponding author on reasonable request.

Conflicts of Interest: The authors declare that they have no known competing financial interests or personal relationships that could have appeared to influence the work reported in this paper.

References

1. Bae, J.H.; Kwak, H.D.; Heo, S.J.; Choi, C.H.; Choi, J.S. Numerical and experimental study of nose for LOx floating ring seal in turbopump. *Aerospace* **2022**, *9*, 667. [CrossRef]
2. Lu, J. Theoretical optimization and experiment on lubrication of floating microgroove cylindrical seal. *Ind. Lubr. Tribol.* **2020**, *72*, 1217–1226. [CrossRef]
3. Li, G.Q.; Zhang, Q.; Huang, E.L.; Lei, Z.J.; Wu, H.W.; Xu, G. Leakage performance of floating ring seal in cold/hot state for aero-engine. *Chinese J. Aeronaut.* **2019**, *32*, 2085–2094. [CrossRef]
4. Wang, L.L.; Guo, S.H.; Wei, Y.L.; Yuan, G.T.; Geng, H. Optimization research on the lubrication characteristics for friction pairs surface of journal bearings with micro texture. *Meccanica* **2019**, *54*, 1135–1148. [CrossRef]
5. Zhai, Z.Y.; Fan, Q.Y.; Qu, Y.J.; Zhang, H.M.; Zhang, Y.C.; Cui, Y.H. Heat transfer mechanism of fiber reinforced composites processed by pulsed laser. *Opt. Laser Eng.* **2023**, *163*, 107473. [CrossRef]
6. Bai, L.Q.; Meng, Y.G.; Khan, Z.A.; Zhang, V. The synergetic effects of surface texturing and MODDP additive applied to ball-on-disk friction subject to both flooded and starved lubrication conditions. *Tribol. Lett.* **2017**, *65*, 163. [CrossRef]
7. Grabon, W.; Pawlus, P.; Wos, S.; Koszelaet, W.; Wieczorowski, M. Effects of cylinder liner surface topography on friction and wear of liner-ring system at low temperature. *Tribol. Int.* **2018**, *121*, 148–160. [CrossRef]
8. Zhao, Z.K.; Shen, Y.; Liu, Y.; Xing, C.F.; Liu, J.; Fan, J.J.; Xu, J.J. Low and high temperature effects on friction and wear performance of Cr-plated cylinder liner. *Wear* **2024**, *546*, 205329. [CrossRef]
9. Li, Y.; Cui, X.; Zhang, J. A study on improving friction and wear performance of bearing bush in radial piston hydraulic motor. *Wear* **2024**, *546*, 205317. [CrossRef]
10. Han, X.; Chen, G.; He, D.; Shan, Y.; Xu, J. Effect of laser surface texturing on the tribological properties and scuffing mechanism of CKS piston ring against cast iron cylinder liner under high intensifying. *Tribol. Trans.* **2022**, *65*, 1149–1159. [CrossRef]
11. Chang, H.C.; Borghesani, P.; Peng, Z.X. Automated assessment of gear wear mechanism and severity using mould images and convolutional neural networks. *Tribol. Int.* **2020**, *147*, 106280. [CrossRef]
12. Zhai, Z.Y.; Rui, R.H.; Tang, A.F.; Zhang, Y.C.; Wang, X.; Cui, Y.H. Fabrication of microstructure on C/SiC surface via femtosecond laser diffraction. *Mater. Lett.* **2021**, *293*, 129711. [CrossRef]
13. Kumar, S.; Choudhary, S.; Khatri, N. Influence of surface texture size and distribution on the friction and wear characteristics of textured surfaces. *Tribol. Trans.* **2019**, 473–487.
14. Wu, J.X.; Deng, J.X.; Bao, Y.C.; Zhang, Z.H. Synergistic effects of heat-assisted ultrasonic rolling textures and self-lubricating coatings on the friction and wear properties of AISI 52100 steel. *Mater. Today Commun.* **2024**, *38*, 108256. [CrossRef]
15. Yang, X.P.; Fu, Y.H.; Ji, J.H. Effect of laser bump texture combination characteristics on friction-wear properties of roll surface. *Ind. Lubr. Tribol.* **2022**, *74*, 522–530. [CrossRef]
16. Elo, R.; Heinrichs, J.; Jacobson, S. Wear protective capacity of tribofilms formed on combustion engine valves with different surface textures. *Wear* **2017**, *376*, 1429–1436. [CrossRef]
17. Yan, W.; Komvopoulos, K. Contact analysis of elastic-plastic fractal surfaces. *J. Appl. Phys.* **1998**, *84*, 3617–3624. [CrossRef]
18. Guan, D.; Jing, L.; Gong, J.; Yang, Z.W.; Shen, H. Friction and wear modeling of rotary disc in spherical pump. *Ind. Lubr. Tribol.* **2019**, *71*, 420–425. [CrossRef]
19. Han, M.; Zhang, J.H.; Dong, P.P.; Du, K.; Zheng, Z.J.; Zhang, C.; Xu, B. Tribological properties and wear mechanism of Ni@Gr reinforced Ni-based alloy coatings prepared via laser cladding. *J. Mater. Res. Technol.* **2024**, *31*, 799–809. [CrossRef]
20. Grill, A. Diamond-like-carbon: State of the art. *Diam. Relat. Mater.* **1999**, *8*, 428–434. [CrossRef]

21. Hong, Y.; Zhang, P.; Lee, K.H.; Lee, C.H. Friction and wear of textured surfaces produced by 3D printing. *Sci. China: Technol. Sci.* **2017**, *60*, 1400–1406. [CrossRef]
22. Markus, S.; Hendrik, W.; Andreas, M. Simulation of wear and effective friction properties of microstructured surfaces. *Wear* **2020**, *464*, 203491.
23. Kai, L.; Zhan, Q.L.; Mashood, A.K.; Chen, L.X.; Zhao, M. Effects of the inclination angles of DLC end face micro-texture on the tribological properties of dry gas seal rings. *Surf. Topogr. Metrol. Prop.* **2021**, *9*, 045014.
24. Zhai, Z.Y.; Wei, C.; Zhang, Y.C.; Cui, Y.H.; Zeng, Q.R. Investigations on the oxidation phenomenon of SiC/SiC fabricated by high repetition frequency femtosecond laser. *Appl. Surf. Sci.* **2020**, *502*, 144131. [CrossRef]
25. Yi, M.Y.; Cheng, J.Z.; Tao, Y.Y. Friction and wear behavior and mechanism of low carbon microalloyed steel containing Nb. *China Foundry* **2023**, *20*, 263–270.
26. Beake, B.D.; Mcmaster, S.J.; Liskiewicz, T.W.; Neville, A. Influence of Si- and W- doping on micro-scale reciprocating wear and impact performance of DLC coatings on hardened steel. *Tribol. Int.* **2021**, *160*, 107063. [CrossRef]
27. Lee, R.S.; Jou, J.L. Application of numerical simulation for wear analysis of warm forging die. *J. Mater. Process. Tech.* **2003**, *140*, 43–48. [CrossRef]